Helmholtz-Zentrum Dresden-Rossendorf (HZDR)

HZDR
HELMHOLTZ ZENTRUM
DRESDEN ROSSENDORF

Terahertz Generation with Ballistic Photodiodes under Pulsed Operation

Müller-Landau, C.; Malzer, S.; Weber, H. B.; Döhler, G. H.; Winnerl, S.; Burke, P.;
Gossard, A. C.; Preu, S.;

Originally published:

October 2018

Semiconductor Science and Technology 33(2018)11, 114015

DOI: https://doi.org/10.1088/1361-6641/aae5e4

Perma-Link to Publication Repository of HZDR:

https://www.hzdr.de/publications/Publ-27967

Release of the secondary publication
on the basis of the German Copyright Law § 38 Section 4.

Terahertz Generation with Ballistic Photodiodes under Pulsed Operation

C. Müller-Landau[1], S. Malzer[1], H.B. Weber[1], G.H. Döhler[2], S. Winnerl,[3] P. Burke[4], A. C. Gossard[4], and S. Preu[5]

[1] Chair of Applied Physics, Friedrich-Alexander University of Erlangen-Nürnberg, D-91058 Erlangen, Germany

[2] Max Planck Institute for the Science of Light, D-91058 Erlangen, Germany

[4] Helmhotz-Zentrum Dresden-Rossendorf, D-01328 Dresden, Germany

[4] Materials Department, University of California, Santa Barbara, California 93106

[5] Dept. of Electrical Engineering and Information Technology, Technische Universität Darmstadt, Germany

E-mail: `preu@imp.tu-darmstadt.de`

Abstract.

We investigate high field and ballistic carrier transport in a 1.55 μm photomixing device based on pin-diodes by time resolved terahertz (THz) spectroscopy. The device consists of 3 stacked In(Al)GaAs pin diodes (n-i-pn-i-p superlattice) attached to a broadband logarithmic-periodic antenna. Each pin diode is optimized for exhibiting ballistic transport and a reduced transit time roll-off. Ballistic transport signatures could be confirmed directly in these experiments. The data are compared with results from continuous-wave (CW) experiments and from simulations both supporting our theoretical expectations. It is demonstrated that n-i-pn-i-p superlattice photomixers are also efficient THz emitters under pulsed operation, showing a maximum THz field strength of ~0.5 V/cm (peak to peak) at 30 mW average optical power.

Keywords: Terahertz generation, ballistic transport, velocity overshoot, photomixer

Submitted to: *Semicond. Sci. Technol.*

1. Introduction

High performance Terahertz (THz) systems nowadays are used in many scientific and industrial applications. THz radiation allows wireless transmission with data rates of 100 Gbit/s [1], spectroscopy and imaging of biological [2] and chemical [3] substances. It can be used for monitoring and quality control in food industry [4]. Broadband THz generation with femtosecond laser pulses in photoconductive semiconductors is a widely used method for these applications. Such systems have already been reported a spectral range from 0.1 THz to 6.5 THz.[5, 6] However, typical time domain THz spectrometers (THz-TDS) only achieve a spectral resolution in the range of 1 to a few GHz [7, 8].
Electronic continuous-wave (CW) systems based on frequency-multiplied microwave sources [9] or quantum cascade lasers (QCLs) [10] offer excellent spectral resolution but only within a narrow frequency window. CW photomixing systems are the most promising approach for high spectral resolution with a wide tunability in the THz-frequency range [11, 12]. The first photomixers have been made from low-temperature gallium arsenide (LT-GaAs) photoconductors operated at 800 nm [13] with μW-level powers under CW operation. Nowadays, specially designed pin diodes for operation at telecom wavelengths like uni-travelling carrier (UTC) diodes [14], use electron transport only and achieved much higher power in the sub-THz range (up to 300 GHz), up to mW level [15, 16], owing to the optimized trade-off between RC-time and transit-time roll-off. At the same time, the n-i-pn-i-p superlattice concept was established [17]. In this approach, the transit time and the RC time can be optimized separately by using a stack of transit time optimized pin diodes. The resulting capacitance, responsible for the RC-time, can be controlled by the number of stacked pin-diodes, leading to an ideal trade-off frequency beyond 1 THz [11, 17, 18]. The key parameter for a short transit time (high 3dB roll-off frequency) is a sufficiently short intrinsic layer allowing for ballistic transport. A thorough analysis of the ballistic electron transport in these structures is required to approve the concept and for optimization.
Time-resolved (pulsed) THz spectroscopy has proven to be a powerful tool to study charge carrier dynamics in GaAs [19], time dependent field screening effects in small-size GaAs-devices [20] and in LT-GaAs [21, 22]. In photoconductive materials, the short life time, $\tau_{rec} < 1$ ps is the reason that scattering dominates the transport and no velocity overshoot has been reported yet [12]. Contrary, in semi-insulating (SI)-GaAs or SI-InGaAs ballistic transport is evident and consequently velocity overshoot. Ballistic electron transport in GaAs THz-emitters has been studied by Monte-Carlo simulations [23] and pump and probe experiments [24]. Furthermore, it has been shown that GaAs/AlGaAs p-i-n heterostructures are efficient pulsed THz emitters, even though they were not designed for ballistic transport [25].
In this paper, we report on time-resolved ballistic transport studies which are compared to CW measurements and simulations. Pulse excitation can create a very high charge carrier density in the n-i-pn-i-p phototomixer and therefore allows to study saturation behaviour and suppression of ballistic transport. Although saturation occurs at fairly

low optical powers, a high conversion efficiency even under pulsed operation could be demonstrated.

2. Carrier transport model

In order to investigate the saturation behavior of photodiodes and determine maximum current densities, we simulate the carrier transport in the device by a simple ballistic 1D transport model where we only account for LO phonon scattering and abrupt inter-valley scattering for electron energies that reach the inter-valley eneregy of $E_{\Gamma L} = 0.55$ eV. Electrons start at zero velocity with purely ballistic transport, with an acceleration of $a = eE/m^*$, where E is the local electric field, e the elementary charge and m^* the effective mass. Phonon scattering has only little impact on the transport at room temperature and in this time regime. Reaching the phonon energy of $E_{LO} = 34$ meV, electrons can emit LO phonons, but the rate for this process is in the ps-range. With higher electron energies phonon scattering becomes more pronounced. When electrons are accelerated up to the inter-valley energy, $E_{\Gamma L} = 0.55$ eV in InGaAs, the onset of intervalley scattering is dominating the scattering processes. At this point electrons find themselves in the (L-)valley at negligible kinetic energy. Here, acceleration starts again but with a substantially higher effective mass and a high rate for scattering into the equivalent side-valleys. This quasi randomizes the direction of carrier motion and finally results in transport at the saturation velocity. For our simulation these processes are simplified as the electrons are assumed to be decelerated instantaneously from the ballistic peak velocity ($\sim 1.4 - 2 \times 10^8$cm/s), to the saturation velocity of 1.3×10^7cm/s [26]. This abrupt transition is a good approximation, since the scattering time is in the range of a few 10 fs, except for extremely low accelerating fields where also only very little THz radiation is generated. We neglect carrier-carrier scattering and alloy scattering as their contributions are only secondary corrections. Holes are considered by a Drude-like acceleration up to the saturation velocity of approximately 5×10^6 cm/s [27]. When the carriers arrive in the highly doped contact, they experience strong scattering and thermalize on a femtosecond time scale. Therefore they are are no longer contributing to the simulation area. The photocurrent density is calculated by adding up the contributions of all carriers, $j = \Sigma_l e n_l v_l$, where n_l is the charge density travelling at velocity v_l. As the n-i-pn-i-p superlattice diode consists of three p-i-n diodes (current sources) connected in series, we allow for a static bias U_{st} to built up due to charge accumulation between the diodes and used it as the only fitting parameter.

The AC current in the pin-diodes creates a field of $E_{THz}(t) \sim \delta j(t)/\delta t$ [2] or going to the frequency domain, $E_{THz}(\omega) \sim i\omega j(\omega)$. The emitted THz-power is $P_{THz}(\omega) \sim \omega^2 j^2(\omega)$. This equation holds for Hertzian dipoles only [28]. When antennas are used, it is more instructive (at least in the frequency domain) to use the concept of radiation resistance as the antenna may strongly alter the emitted spectrum. For the case of a Hertzian dipole, the radiation resistance is $R_{rad} \sim \omega^2$ [28]. Replacing the Hertzian dipole radiation resistance by the radiation resistance of the antenna, the

emitted power can be denoted as $P(\omega) = \frac{1}{2} R_{rad} j^2(\omega) A^2$, where A is the cross section of the device. In the experiment, we use a broadband, self-complementary logarithmic periodic antenna that shows only little frequency dependence of the real part and almost negligible imaginary part, at least below 800 GHz where most of the power is measured. Above 800 GHz, the antenna performance decreases, confirmed by simulations. In contrast to the Hertzian dipole with a $R_{rad} \sim \omega^2$-dependence (originating from the time derivative), we consider for the logarithmic-periodic antenna a constant resistance $R_{rad} = 70\ \Omega$ where the emitted THz field is directly proportional to the photocurrent. The generated THz spectra are filtered by the RC roll-off due to the antenna (R) and device capacitance (C) with an onset at $f_{3dB}^{RC} = 150$ GHz. For pulsed measurements, a further high pass roll-off attributed to the electro-optic sampling (EOS) detection technique arises: The lower the THz frequency, the larger the THz spot and therefore the lower the overlap between THz and laser beam in the detection crystal. This results in a high pass behavior which is fitted to a cut-off frequency of 400±100 GHz.

3. Pulsed THz emission with pin diodes

The setup for pulsed measurements consists of a Toptica FFS 1550 nm mode-locked fiber laser, with a repetition rate of 78 MHz, a pulse duration of 100 fs and a maximum optical power of 100 mW. A part of the laser beam illuminates the device through a lens with a focal length of 15 cm. The device is with about 80 μm^2 much smaller than the expected spot size given by the numerical aperture of the lens, resulting in a homogeneous, plane-wave illumination and an approximately constant carrier concentration within its cross section. The device is a three-period n-i-pn-i-p superlattice photomixer [18] with an intrinsic layer thickness of 150 nm comprising a linear grading from $In_{0.53}Ga_{0.47}As$ to $In_{0.53}Al_{0.08}Ga_{0.39}As$, followed by a 50 nm $In_{0.53}Al_{0.08}Ga_{0.39}As$ transport layer. The majority of the carriers is generated in the first $\sim$ 50 nm of the graded layer.At the interface of the diodes, a quasi-metallic ErAs-layer is implemented to ensure a high current censity [29] and little loss of RF power. The generated current is then fed into a broadband, logarithmic-periodic antenna with a bandwidth of $\sim$ 60 GHz-2 THz. The THz beam is imaged by a silicon lens (diameter 10 mm, hyperhemispherical offset 1 mm) followed by two off-axis parabolic mirrors on a ZnTe crystal.

The second part of the laser beam is frequency-doubled and then combined with the THz signal for electro-optic detection in the ZnTe crystal. A set of balanced photodiodes reads out the THz-induced electro-optic effect in the crystal, which is the measure for the THz field strength. We used lock-in technique to improve the signal to noise ratio. An accousto-optic modulator working at 89.05 kHz chopped the laser signal exciting the photomixer. . The time domain traces at several biases were measured first in order to confirm that the position of the peak does not change. These traces are also used for the frequency domain evaluation. Accordingly, the time delay is adjusted for a maximum THz field strength, E_{pk} in the time domain vs. bias. Fig. 1 a) shows the normalized peak THz power, $P_{pk} \sim E_{pk}^2$ vs. DC bias. For low carrier density

($n^{(2D)} \leq 4 \times 10^{11}$A/cm^2), the power-voltage characteristics shows a pronounced peak. This feature already proves a major signal contribution from the ballistic transport since it is strongly field-dependent [17] while transport at saturation velocity would not show a field-dependence in the region beyond a few tens of kV/cm without any peak signature. We note that for pulses much shorter than the transit-time, the structure of the peak field, E_{pk}, vs. bias resembles that of the average carrier velocity, v_{av}^{tr} vs. bias as $E_{pk}(U_{DC}) \sim j(U_{DC}) \sim env_{av}^{tr}(U_{DC}) \sim v_{av}^{tr}(U_{DC})$, while the carrier concentration, $n \sim P_L$, can be considered as a delta-shaped pulse in the time domain with all carriers generated within the same time slot. For our case, however, the pulse duration of 100 fs is already a large fraction of the transit time (≈200 fs), blurring this relation, as separation of early generated carriers starts to screen the built-in field for subsequently generated carriers. Fig. 1 a) also shows simulation results without any scaling. The only

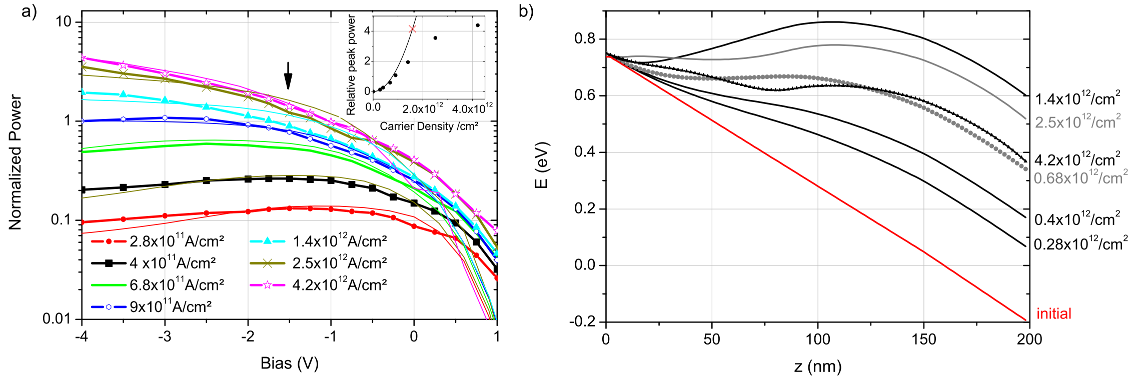

Fig. 1. a) THz peak power vs. bias. Thick lines: experiment, thin lines: simulation. Both experimental and theoretical powers are normalized to the power at $n^{(2D)} = 9 \times 10^{11}$A/cm^2 and $U_{DC} = -4$ V for comparison. The inset shows the saturation of the peak power vs. carriers per pulse (points). Unsaturated detectors would show the depicted parabolic increase (solid line) of power with carrier density. The carrier density of 1.58×10^{12} /cm^2 where the power is reduced by 3 dB is marked by the red cross. b) Saturation of the photodiode. The built-in field is inhomogeneously screened at high laser powers. The simulated results are taken for a Gaussian pulse of 100 fs duration at a time of 100 fs after the peak for an internal (accelerating) reverse bias of -0.2 V (-1.5V external bias for the three period device, indicated by the arrow in (a)).

fitting parameter of the simulation is the initially screened bias due to the superlattice structure, $U_{scr} = 0.3V$/period in order to match theoretical and experimental bias for optimum performance at low optical powers. There is excellent agreement between experiment and theory both in terms of shape and (relative) emitted THz power vs. bias for a photocurrent range of more than one order of magnitude. Only in the forward direction, i.e. at very low electric fields, we see some discrepancy. This is most likely due to the simplifying assumption that carriers scatter immediately into the side-valley once reaching the inter-valley energy, $E_{\Gamma L}$ with an instantaneous decrease of the velocity to the saturation velocity.

From the simulations, we determine an optimum field for pulsed operation for the

lowest experimentally investigated carrier density of 2.8×10^{11}A/cm^2 of 47 ± 3 kV/cm. This optimum field strength is about 30% higher than the field strength of 35 kV/cm that delivers the shortest ballistic transit-times (around 230 fs) in the simulation at vanishing carrier density (c.f. Fig. 2 a), inset), indicating that the applied field is already screened to some amount. The deformation of the band structure by screening of carriers as illustrated in Fig. 1 b) for 100 fs after the maximum optical excitation. It reveals that already these low carrier densities generate a field screening of 10-15 kV/cm. A higher external reverse bias is therefore necessary to restore the optimum transport condition. At higher photocarrier densities, however, the potential becomes so strongly distorted that the transport across the whole intrinsic layer is far from optimum. Ballistic overshoot may even result in a field opposing the built-in field within the intrinsic layer as shown in Fig. 1 b) for a simulated carrier density of 1.4×10^{12} /cm^2. If the field is far from optimum for ballistic transport the peak height in Fig. 1 a) is reduced and shifted to higher negative bias. At the highest photocurrents, screening appears at time scales of a few 10 fs, reducing the average carrier acceleration and their separation for subsequent time steps. This, in turn, reduces the strength of screening and explains the less distorted band at the highest investigated current densities. Here, the electric field is very low at the beginning of the intrinsic layer, where most of the carriers are situated. The low field, however, strongly increases the transit-time and the THz output of the device saturates. Even higher laser power does not notably increase the THz output as shown for the highest investigated carrier densities of 2.5×10^{12} and 4.2×10^{12} /cm^2 as shown in the inset of Fig. 1 a). Such early saturation is indeed expected for pin diodes where all generated carriers contribute to the photocurrent. Compared to photoconductors, where only a small fraction (i.e. the gain, $g \sim 0.1\%$) contributes to the photocurrent, screening is far less pronounced [12]. Therefore, photoconductors are typically used in pulse experiments, while pin diodes are much more powerful sources in CW setups where their output power benefits from the large photocurrent while screening is much less severe due to the much smaller peak photocurrent densities. Remarkably, in the n-i-pn-i-p superlattice photomixers we achieved with a photocurrent as low as 4.2 μA (carrier density of 4.2×10^{11} A/cm^2) a peak to peak THz field strength of 0.47 V/cm. This field strength is comparable to results obtained with 1550 nm compatible large area photoconductive emitters (LAE) [30, 31], although the absorbed laser power is about three orders of magnitude higher than in the n-i-pn-i-p superlattice photomixer.

Fig. 2 a) shows the spectrum generated by the pin diode and detected with EOS at an intermediate current density of 6×10^{11}A/cm^2. There is excellent agreement between simulation and theory, however, with the exception of a slightly stronger roll-off towards high frequencies. This is partly due to the degraded antenna performance above 0.8 THz but also indicates that the simulated transit time, shown in the inset, may be shorter than that in the experimental results.

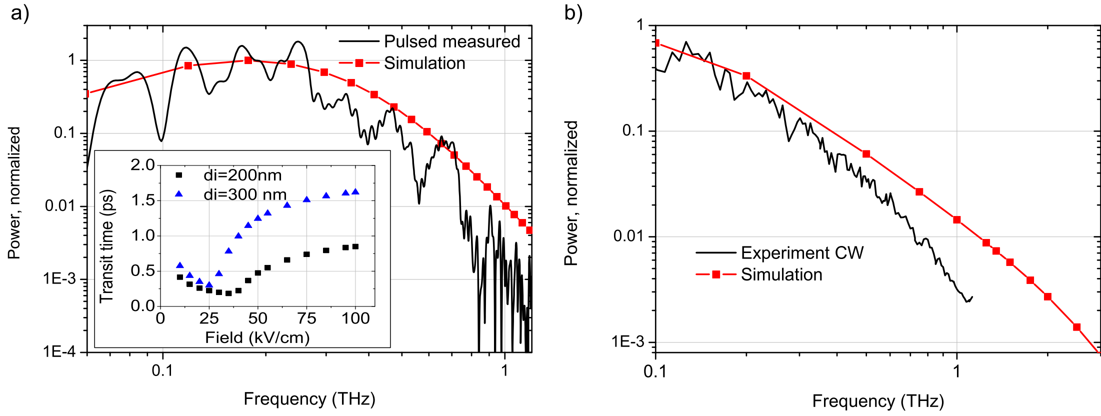

Fig. 2. a) Solid black line: Experimentally obtained pulsed spectrum at a reverse bias of -1.5V and a carrier density of 6×10^{11}A/cm^2. Red line with symbols: simulated spectrum. Inset: simulated transit times for the unsaturated case of a diode with a total intrinsic layer of length 200 nm as described in the text and a longer diode with 300 nm (150 nm grading, 150 nm transport length). b) Measured and simulated spectra for CW operation for a photocarrier density of 3.75 kA/cm^2 under optimum transport conditions, normalized to the power at $f \to 0$ Hz.

4. Ballistic transport under continuous-wave operation

It is well known that ballistic contributions enhance the THz power of continuous-wave (CW) operated pin based photomixers [17]. However, quantitative studies for 1550 nm operated devices are missing; to the knowledge of the authors, only ballistic transport in GaAs-based devices has been directly investigated [23]. Therefore, a similar device as for the pulsed measurements is characterized in a 1550 nm CW photomixing setup, consisting of two DFB laser diodes that are combined and subsequently amplified by an erbium doped fiber amplifier. The THz signal is collimated by a silicon lens mounted on the backside of the sample, followed by two parabolic mirrors, that image the THz signal on a Golay cell detector. One laser signal is mechanically chopped for lock-in detection. The photocurrent density is 3.75 kA/cm^2, a value where little saturation is expected as confirmed by simulations. The single frequency operation under CW conditions allows to frequency-resolve the emitted power vs. bias with the (almost) frequency independent Golay cell detector. Fig. 3 a) depicts a measurement of THz power vs. bias, featuring a similar peak structure with a pronounced optimum bias as in the pulsed measurements. This proves again ballistic contributions to the transport, enhancing the transit-time 3 dB frequency at optimum transport conditions. At low frequencies ($f_{THz} \ll 0.66$ THz), the peak becomes less pronounced since transport at saturation velocity is sufficient to separate electrons from holes on a time scale of $1/(2f_{THz})$. Interestingly, the peak also becomes less pronounced for frequencies above 0.66 THz as shown by the inset of Fig. 3 a). This clearly contradicts the expectation of the classical roll-off equation,

$$\eta_{tr}^{class}(f, f_{tr}^{3dB}) = \frac{1}{1 + (f/f_{tr}^{3dB})^2}, \qquad (1)$$

with $f_{tr}^{3dB} \approx 0.5/(\tau_{tr})$ [11]. While the optimum bias yields the shortest transit time, τ_{tr}^{opt}, a strong reverse bias increases the transit time severely, as shown in the inset of Fig. 2 a). At frequencies (much) above the transit-time 3 dB frequency for optimum transport, the THz power at optimum bias according to Eq. 1 (normalized to that of a high reverse bias) saturates at a value of $(\tau_{tr}(-2V)/\tau_{tr}^{opt})^2$, where $\tau_{tr}(-2V)$ is the transit time at the reverse bias of -2V in the n-i-pn-i-p superlattice photomixer used in this experiment.

This is not reproduced by the experiment that shows a pronounced peak. Actually, Eqn. (1) is only an approximative solution for frequencies below the transit-time 3 dB frequency as shown in ref. [11]. Above the transit-time 3 dB frequency, the performance strongly depends on the actual carrier transport (ballistic contributions vs. transport at saturation velocity) and the potential shape of the absorption region. Therefore, the frequently used Eqn. (1) describes the transit-time roll-off behavior of the diode above its 3 dB frequency inadequately and cannot be used to derive the transit-time. We note that the measurement of the power-voltage charateristics yields much higher accuracy on the optimum transport field than fits of the transit-time 3 dB frequency of the measured spectra. The latter are prone to alignment errors, distortion by the diffraction limit at low frequencies, or antenna emission efficiency and radiation resistance, resulting in substantial errors. In contrast, power-voltage characteristics as shown in Fig. 3 a) cancel all setup-specific dependencies since only relative power values are relevant and therefore are well suited to examine ballistic performance and determine the optimum transport field.

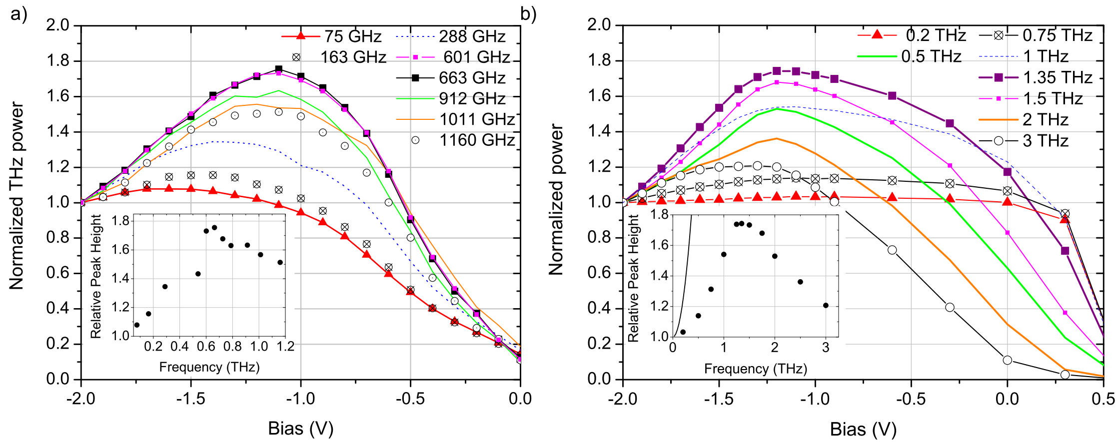

Fig. 3. a) Measured power-voltage characteristics for various frequencies under CW operation. Inset: extracted peak enhancement, normalized to the power at U=-2V. b) Simulation results for the same structure. Inset: peak height normalized to the power at U=-2V (symbols) including the expectation for the simplified roll-off by Eqn. (1) as solid line.

Fig. 3 b) shows simulation results for the diode. Both peak structure and general frequency-dependent behavior show excellent qualitative agreement. However, the peak in the simulations appears at about two times higher frequency. Further, the

experimentally fitted transit-time 3 dB frequency of ∼0.55±0.1 THz is about three times lower than the 3 dB frequency of 1.7 THz fitted to the simulated spectrum as shown by the spectra in Fig. 2 b). The measured spectrum, however, depends strongly on the antenna performance. From RF simulations, we determined that the antenna efficiency of the logartihmic-periodic antenna starts to decrease above ∼ 800 GHz because it is perturbed by the photomixer and sample geometry. Another sample, equipped with a logarithmic-periodic spiral antenna showed a fitted transit-time 3 dB frequency of 0.85 ± 0.15 THz. Still, the experimentally fitted transit-time 3 dB frequency is lower than the simulated one. Even if further scattering mechanisms are included in the simulations to describe for the deceleration of carriers, this not sufficient to explain this discrepancy. If electron-electron scattering is "'switched on"', it should substantially increase the probability of inter-valley scattering and increase the transit-time towards the experimentally observed values. This may also have an impact on the optimum transport field. Despite this discrepancies, the simulation results allow for qualitative conclusions: The largest peak height usually appears at frequencies lower than the transit-time 3 dB frequency, i.e. defining a lower boundary for the transit-time 3 dB frequency. An exact relation, however, cannot be specified since it depends also on the reverse bias used for normalization. Here, the simulated peak of the power-voltage characteristics is at 1.35 THz, while the fitted 3 dB frequency of the measured data is at 1.7 THz, i.e. 25% higher. From the measured power-voltage characteristics with a peak at 0.66 THz we conclude that the transit-time 3 dB frequency of the device is around 0.83 THz, in excellent agreement with the fitted transit-time 3 dB frequency of 0.85 THz from the logarithmic-periodic antenna. The simulations further allow to analyze the shape of the spectrum emitted by a pin diode photomixer and deduce improved expressions for the transit-time. In most publications, the transit-time 3 dB frequency is approximated as $f_{tr}^{3dB} \approx 0.5/(\tau_{tr})$. In ref. [11] we already found that this approximate description does not adequately describe the frequency characteristics. With some simplifying assumptions on the transport, we obtained an analytical 3 dB frequency for ballistic transport of $f_{bal}^{3dB} \approx 0.55/(\tau_{tr})$ and $f_{sat}^{3dB} \approx 0.44/(\tau_{tr})$ for saturation transport. These 3 dB frequencies, however, only describe the frequency dependence well below the 3 dB frequency. From the simulation results obtained in this paper, a better overall agreement is obtained for $f_{tr}^{3dB} \approx 0.4/\tau_{tr}$, i.e. higher frequencies are substantially stronger suppressed than frequencies below the 3 dB frequency, where Eqn. (1) is still a good approximation. Therefore, the transit-time 3 dB frequency fitted to the simulated spectra is 1.7 THz for a transit time of 0.23 fs.

5. Conclusions

We have examined the impact of ballistic transport on THz emission in n-i-pn-i-p superlattice photomixers under pulsed and CW excitation experimentally and by numerical studies for both types of excitation. The numerical studies generally underestimate ballistic transit times, but allow for many qualitative predictions. The

appearance of a peak in the THz power-voltage characteristics was well reproduced for proving ballistic transport within the diodes. The frequency dependence of the power-voltage characteristics allows for conclusions on the transit-time of the electrons within the device and further shows that the usual roll-off expression inadequately describes the THz-spectra generated by pin diodes. The experimental results show that n-i-pn-i-p photomixers are very efficient THz emitters, even under pulsed emission. If a pin diode or a n-i-pn-i-p superlattice photomixer could be implemented in a large area configuration [33], where the laser power is distributed over a large area in order to prevent local saturation by carrier screening, such devices could become very powerful pulsed THz sources.

References

[1] Koenig S, Lopez-Diaz D, Antes J, Boes F, Henneberger R, Leuther A, Tessmann A, Schmogrow R, Hillerkuss D, Palmer R, Zwick T, Koos C, Freude W, Ambacher O, Leuthold J and Kallfass I 2013 *Nature Photonics* **7**, 977-981

[2] Jepsen P, Cooke D G and Koch M 2011 *Laser Phot.* **5** 124–166

[3] McIntosh A I, Yang B, Goldup S M, Watkinson M and Donnan R S 2012 *Chemical Society Reviews* **41** 2072–2082

[4] Gowen A, Osullivan C and ODonnell C 2012 *Trends in Food Science & Technology* **25** 40–46

[5] Nandi U, Norman J C, Gossard A C, Lu H and Preu S 2017 *J. Infrared Mill Terahz Waves* **39** 340–348

[6] Globisch B, Dietz R, Kohlhaas R, Göbel T, Schell M, Alcer D, Semtsiv M and Masselink W 2017 *Journal of Applied Physics* **121** 053102

[7] Klatt G, Gebs R, Janke C, Dekorsy T and Bartels A 2009 *Opt. Express* **17** 22847–22854

[8] Harmon S A and Cheville R A 2004 *Appl. Phys. Lett.* **85** 2128–2130

[9] Neese C F, Medvedev I R, Plummer G M, Frank A J, Ball C D and De Lucia F C 2012 *IEEE Sensors Journal* **12** 2565–2574

[10] Müller A and Faist J 2012 *Nature Photon.* **4** 291

[11] Preu S, Döhler G H, Malzer S, Wang L and Gossard A C 2011 *J. Appl. Phys.* **109** 061301

[12] Carpintero G, Garcia-Munoz L, Hartnagel H, Preu S and Räisänen A 2015 *Semiconductor THz Technology: devices and systems for room temperature operation* 1st ed (New York: John Wiley & Sons)

[13] Brown E R, McIntosh K A, Nichols K B and Dennis C L 1995 *Appl. Phys. Lett.* **66** 285–287

[14] Ito H, Nakajima F, Futura T and Ishibashi T 2005 *Semicond. Sci. Technol.* **20** 191–198

[15] Ito H, Hirata A, Minotani T, Sasaki A, Hirota Y and Ishibasi T 2003 *IEEE Proc.-Optoelectron.* **150** 138–142

[16] Rymanov V, Stöhr A, Dülme S and Tekin T 2014 *Optics Express* **22** 7550

[17] Döhler G H, Renner F, Klar O, Eckardt M, Schwanhäußer A, Malzer S, Driscoll D, Hanson M, Gossard A C, Loata G, Löffler T and Roskos H 2005 *Semicond. Sci. Technol.* **20** 178–190

[18] Preu S, Renner F H, Malzer S, Döhler G H, Wang L J, Wilkinson T L J, Brown E R, Hanson M and Gossard A C 2007 *Appl. Phys. Lett.* **90** 212115

[19] Ulbricht R, Hendry E, Shan J, Heinz T F and Bonn M 2011 *Reviews of Modern Physics* **83** 543

[20] Wang T, Yang Z, Zou S, Wang K, Wang S, and Liu J 2015*Front. Optoelectron.* **8** 98–103

[21] Segschneider G, Jacob F, Löffler T, Roskos H G, Tautz S, Kiesel P and Döhler G 2002 *Physical Review B* **65** 125205

[22] Awad M, Nagel M, Kurz H, Herfort J and Ploog K 2007 *Appl. Phys. Lett.* **91** 181124

[23] Schwanhäußer A, Betz M, Eckardt M, Trumm S, Robledo L, Malzer S, Leitenstorfer A and Döhler G H 2004 *Phys. Rev. B* **70** 085211

[24] Betz M, Trumm S, Sotier F, Leitenstorfer A, Schwanhöußer A, Eckardt M, Schmidt O, Malzer S, Döhler G H, and Hanson M 2004 *Semiconductor Science and Technology* **19** 167–169

[25] Lisauskas A, Reklaitis A, Venckevičius R, Kašalynas I, Valušis G, Grigaliūnaitė-Vonsevičienė G, Maestre H, Schmidt J, Blank V, Thomson M, Roskos H and Köhler K 2011 *Applied Physics Letters* **98** 091103

[26] VBalynas, AKrotkus, AStalnionis, ATGorelionok, NMShmidt and JATellefsen 1990 *Appl. Phys.A* **51** 357–360

[27] SAdachi 1992 *Physical Properties of III-V Semiconductor compounds* (John Wiley and Sons)

[28] Preu S 2014 *Journal of Infrared, Millimeter, and Terahertz Waves* **35** 998–1010

[29] Preu S, Malzer S, Döhler G H, Lu H, Gossard A C and Wang L J 2010 *Submitted to Semicon. Sci. Technol.*

[30] Preu S, Mittendorff M, Lu H, Weber H, Winnerl S and Gossard A 2012 *Appl. Phys. Lett.* **101** 101105

[31] Xu M, Mittendorff M, Dietz R J B, Künzel H, Sartorius B, Göbel T, Schneider H, Helm M and Winnerl S 2013 *Appl. Phys. Lett.* **103** 251114

[32] Beck M, Schäfer H, Klatt G, Demsar J, Winnerl S, Helm M and Dekorsy T 2010 *Opt. Express* **18** 9251–9257

[33] Döhler G H, Garcia-Munoz L E, Preu S, Malzer S, Bauerschmidt S, Montero-de Paz J, Ugarte-Munoz E, Rivera-Lavado A, Gonzalez-Posadas V and Segovia-Vargas D 2013 *IEEE Transactions on Terahertz Science and Technology* **3** 532–544